On the mechanical response in nanoalloys: the case of NiCo

Juan A. de la Rosa Abad[1], Eduardo M. Bringa[2], Sergio J. Mejía-Rosales[3] and Marcelo M. Mariscal[1]

[1] INFIQC, CONICET, Departamento de Química Teórica y Computacional, Facultad de Ciencias Químicas, Universidad Nacional de Córdoba, Córdoba 5000, Argentina.
[2] CONICET and Facultad de Ingeniería, Universidad de Mendoza, Mendoza 5500, Argentina; Centro de Nanotecnología Aplicada, Facultad de Ciencias, Universidad Mayor, Santiago 8580745, Chile.
[3] Centro de Investigación en Ciencias Físico-Matemáticas (CICFIM), Facultad de Ciencias Físico-Matemáticas, Universidad Autónoma de Nuevo León, San Nicolás de los Garza, Nuevo León 66455, México.

Abstract

In this work, nanoindentation of spherical NiCo nanoalloys with core-shell and random mixing patterns was studied, and we compared them against monometallic nanoparticles in order to investigate how the mechanical response may be influenced by the elemental distribution and the proportion of each element. Independently of the mixing patterns, plasticity begins with the nucleation of Shockley partial dislocations (SPD) at the nanoparticle surface, on several slip planes, which leads to the appearance of sessile dislocations and either a stacking fault pyramid (SFP) or an open pyramid at the poles of the spherical nanoalloys. SPDs leave behind stacking faults but, for core-shell structures, the formation of nanotwins was also observed. It was also found that the presence of Co in the external shell of the nanoparticle has the effect of raising the yield strength, which could be interpreted in terms of unstable stacking fault energy. These results have relevance in the design of nanoalloys, since elemental distribution and stoichiometry can be used to tune the desired mechanical properties of the nanoparticle.

INTRODUCTION

The controlled synthesis of alloys at the nanoscale broadens the range of possibilities for the use of this kind of nanostructures in electronics, catalysis, and sensing. For any of these modern applications mechanical properties become an important issue, since nanostructures have to endure thermal and mechanical loads without compromising the structural stability and the performance of the devices.

The ability to produce stronger materials with higher fracture toughness is a challenge in materials science from decades ago. In this sense, pure metals are usually strong but ductile, which means that their ultimate strength may be high, but at the same time they experience irreversible plastic deformation which leads to relatively low fracture strain. However, mixing two or more metals in segregated or mixed patterns appears as a promising approach to overcome that problem.

The mechanical processes at the atomistic level involved in the deformation of a multi-metallic nanoparticle not only depend on the composition, but the specific

distribution of the elements may have a substantial effect in the way particles react to an external stress. This, and the now well-established fact that the reduction in the dimensions of a material improves the mechanical response[1,2] remarks the importance of developing robust techniques that contribute to the understanding of the deformation processes involved in the mechanical response in nanoalloys.

Early experimental work on the compression of monocrystalline Au nanoparticles shows a clear dependence of the yield strength on the size of the nanoparticles[3]. Size effect in compression of single-crystal gold microparticles. They found that the smaller microparticles yield at higher compressive stresses. Since detailed experimental investigation of the atomistic processes behind this behavior is limited, a set of molecular dynamics was implemented, scaling the size of the particles and speeding the compression process; the simulations show that the deformation is driven by the nucleation of dislocations at the surface of the nanoparticles. In contrast, Kiani *et al.*[4], using a combined experimental-simulation approach, show that in bimetallic core-shell nanoparticles the role of the interface may have an effect in the way dislocations nucleate and promote deformation: in Au-core/Ag-shell nanoparticles, dislocations nucleated at the surface traverse the core-shell interface, while in Au(core)/Cu(shell), with defects at the Au/Cu interface, dislocations extend from the interface to the surface, and the particles show hardening after yield. These results are particularly important because experimental procedures allow the synthesis of a large range of bimetallic core-shell nanoparticles. In a recent paper, we have investigated the mechanical response of Au/Pd core-shell cubic nanoparticles, showing that, unlike pure Pd particles, the nucleation of dislocations starts at the semicoherent Au−Pd interface, producing a reduction in the nanocube's strength[5].

These improved mechanical properties found in metallic NPs, makes them very interesting for enhancing the thermomechanical properties of lubricants, as well as for strengthening nanocomposite materials in general.

For crystalline metal NPs, the formation of partial dislocations inside the NPs have been demonstrated as one of the main factors to produce changes in the mechanical behavior of NPs, which contrast with the previously assumed concept that no dislocations are present in crystalline NPs[6].

Nickel-base alloys have been used for several decades in industrial applications where operation conditions involve high stress, high temperature, or corrosive atmospheres, such as aircraft turbines, nuclear power systems, and equipment exposed to heat[7]. At the nanoscopic level, it has been found experimentally that Ni nanoparticles exhibit an unusually high compressive strength of up to 34 GPa, and these results have been confirmed using molecular dynamics simulations where Wulff polyhedral nanoparticles were first rounded to mimic the shape the experimental systems[8]. The simulations show that, under compression, failure is triggered by the nucleation of Shockley partial dislocations at the particle corners, followed by an homogeneous dislocation nucleation inside the particle. Geometry also plays a central role in the dynamics of dislocations in the plastic regime: Molecular dynamics simulations of the compression of copper spherical

nanoparticles show that after the elastic response, dislocations are nucleated at the edges in contact with the plane indenters performing the compression; this leads to the formation of a pyramidal dislocation structure[9]. The formation of these kinds of pyramidal structures has been reported also in the compression of spherical Ni nanoparticles[10].

In the case of bimetallic NPs, an important aspect to evaluate is related to how the distribution and amount of each constituent element can affect the mechanical properties of nanomaterials. In this sense, it is important to understand if the interface formed by the junction of two surfaces of different chemical nature (i.e. different lattice parameter, cohesive energy, surface energy, etc) in the case of core-shell configuration, can play an important role in the development of partial dislocations through the material; or if the random mixing of the elements changes the way dislocations are generated and/or propagated inside the material.

Understanding the main mechanical properties of nanoalloys, such as the hardness, Young modulus and dislocation dynamics, will aid in the rational design of nanoalloys for specific applications. In this paper, we present an analysis of the structure and dynamics of CoNi nanoparticles under compression obtained from a set of molecular dynamics simulations, making a special emphasis in the methodology followed to investigate the nucleation and nature of dislocations, and the generation of stacking faults and twins in monometallic, core-shell, and randomly alloyed nanoparticles.

METHODS AND MODELS

Spherical nanoparticles (NP) made of Ni and Co were indented using classical molecular dynamics simulations. In this study, we explore pure Co and Ni NPs, as well as mixed (random) and core-shell distributions with several compositions. In the core-shell distribution, the core could be either Ni or Co. For each distribution, the elemental proportions explored were 12.5, 25, and 50 % of the total number of atoms in the nanoparticle. In order to compare the effect of the elemental distribution within the nanoalloy, random distributions with the same elemental proportions were studied; for all cases, fifteen MD simulations were made for each setup in order to have a set of results statistically sound. In the present study, the diameter of the nanoalloys was set to 9.7 nm, well within the range of sizes of typical experimentally synthesized NPs. As a notation, we will use the first element as the core and the second as the shell; for example, CoNi means that the Co is present in the core and Ni in the shell.

The large-scale atomic/molecular massively molecular simulator (LAMMPS) simulation code[11], with the GPU package[12], was used to perform the MD simulations. An Embedded Atom Model (EAM) potential due to Li, Sheng and Ma[13] was used to describe the interaction between atoms. The dynamical trajectories of the atoms were analyzed using the Ovito visualization software[14]. As implemented in Ovito, the crystal structure was determined using Polyhedral Template Matching[15] (PTM), with

rmsd=0.1, and the Burgers´ vectors and dislocation lines were determined using the Dislocation eXtraction Algorithm (DXA)[16].

All atoms were placed onto an ideal fcc lattice, and initial atomic positions were relaxed before nanoindentation, using a conjugate gradient minimization with tolerance energy and force of 10^{-12} eV and 10^{-12} eV/Å, respectively. Subsequently, the nanoparticles were thermalized at 300 K during 4 ns using a Nosé-Hoover thermostat with a damping parameter of 0.1 ps in an NVT ensemble. This procedure ensured stress relaxation, leading to negligible global stress for the NP before indentation. The timestep used in each simulation was 2 fs. After thermalization, an external repulsive force was applied to the NP through two flat indenters. Depending on the indenter position R, the force is described as:

$F(r) = -K (r- R)^2$ for r >= R,

$F(r) = 0$ for r < R,

where K is the indenter constant, and the distance between the atom and indenter position is r-R. The K value of the indenter was chosen to be 10 eV/A^3, and 2 m/s is the velocity of one indenter, corresponding to a strain rate of approximately $2x10^8$ s^{-1}, which may be considered high when compared against experiments, but that is nevertheless within the strain rate range typically used in molecular dynamics compression processes, usually in the 10^7-10^9 s^{-1} range[17]. The other indenter stays fixed, in order to mimic a substrate surface to support the nanoalloy. The indentation is along the [001] direction, and, due to the way the sphere was carved from an fcc lattice, the nanoparticle exposes to the indenter a small island with a (100) top face. The initial indenter position is slightly above the nanoparticle, such that the initial force is zero. The total indentation time was 0.6 ns. The yield stress is calculated as σ_y = f/A, where f is the force exerted by the mobile indenter just before a dislocation is nucleated, and A is the cross-section area of the nanoparticle in contact with the mobile indenter at that point. In order to calculate this area, a single layer of atoms close to the indeter was considered, and the area covered by each single atom in the contact plane was assumed to be d^2= 6.17 $Å^2$, for *d* equal to the nearest neighbor distance on the (001) plane.

RESULTS AND DISCUSSION

The deformation mechanisms of pure Co and Ni NPs, as well core-shell and mixed alloys were studied at the atomistic level through the analysis of the MD trajectories during the compression process. The longitudinal engineering strain was calculated here by measuring the distance between the indenters. The mechanical response of pure Co, Ni, core−shell and mixed alloys, with different composition (A:12.5%-B:87.5%, A:25%-B:75%, and A:50%-B:50%) was calculated, where A and B could be both, Co or Ni. As an example, in Figure 1, the force vs longitudinal strain curves are shown for 50%-50% composition (i.e. core-shell: $Co_{50}Ni_{50}$, $Ni_{50}Co_{50}$ and random mix $Co_{50}Ni_{50}$). The curves for the monometallic Co and Ni NPs are also shown. As expected[10,17], a serrated behavior is found in all cases, with a strong

correlation between jumps in the force curve and the nucleation of partial dislocations discussed below. It can be noted in the figure that core-shell particles sustain their elastic behavior at values of strain that lay between those of the Co monometallic NP (yield at strain of 3.64%) and the Ni monometallic NP (yield at strain of 4.42%); in particular, the comparison of the stress-strain curve in (c) against the one in (a) shows that the Ni shell contributes to improve slightly the resistance of the core-shell nanoparticle to plastic deformation. In contrast with this, the completely alloyed CoNi nanoparticle requires a smaller amount of stress to be permanently deformed. The results obtained for other compositions are shown in Supplementary Information but similar behavior is observed.

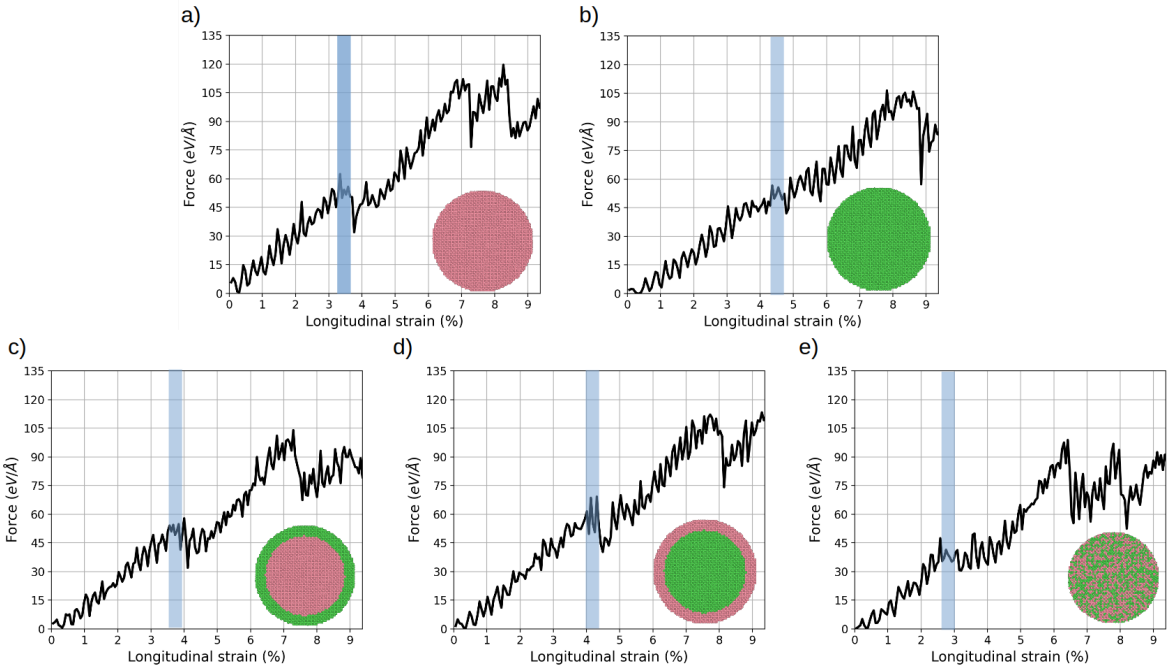

Figure 1. Force vs longitudinal strain curves for five different nanoparticles showing the elastic-plastic transition in each case as a blue stripe. Elastic-plastic transition longitudinal strain is given for each case. (a) Monometallic Co NP, 3.64 %; (b) monometallic Ni, 4.42%; (c) core-shell $Co_{50}Ni_{50}$, 3.89%; (d) core-shell $Ni_{50}Co_{50}$, 4.19%; and (e) random mixed $Co_{50}Ni_{50}$, 2.86%. Insets show elemental distributions in the sliced nanoparticles. The pink and green spheres represent Co and Ni atoms, respectively.

Yield strength is the maximum stress that can be sustained in a material without causing plastic deformation and, consequently, it is very important in the production processes used for many materials such as pressing and rolling, among many others. For these NP, plasticity is associated with dislocation generation, and yield strength can be extracted from the stress-strain curves together with a dislocation density analysis. Figure 2a shows how the yield strength is affected when changing the elemental composition and mixing pattern for CoNi, NiCo and random mixed nanoalloys, and at the same time it is compared with those values calculated for the monometallic ones. Yield strength is plotted against either the percentage of atoms that form the core in core-shell nanoparticles, or as the percentage of Co atoms (blue dots) or Ni atoms (orange dots) in NP where the chemical species are

randomly distributed in the whole volume of the NP. This choice for presenting the results was made in order to have a way to compare NP with the same overall composition. NiCo core-shell nanoalloys present higher yield strength, which could be understood in terms of the unstable stacking fault energy (USFE)[18–20] , as it is shown in Figure 2b. A group of atoms have to overcome the energy barrier given by the USFE in order to displace atomic planes and generate a partial dislocation which will leave a stacking fault behind. In pure Co this barrier is higher than in Ni or in NiCo alloys. Dislocations start at the surface and, therefore, dislocation nucleation is controlled by the shell in core-shell NPs. As a result, it can be understood that the pure Co NP has a higher yield strength than the pure Ni NP, and that the NP with a pure Co shell are the hardest ones. We note that the SFE surfaces in Fig. 2b agree well with the ones presented as a result of empirical potential development.[13]

The pure Ni NP has a high strength close to 19 GPa, but much lower than the one reported for Ni NP[8] compressed along [111], which is expected partly due to the compression along the closed-packed direction. It must be noted, however, that a larger stress estimate (22.5 GPa) is obtained normalizing the contact force with the area of contact at nearly zero strain, as it was done in ref. [8].

For random mixed nanoalloys, Figure 2b shows that the barrier increases going from 25% to 75% Co. This is consistent with the yield strength increase in Figure 2a. 75% Co would be equivalent to 25% Ni_xCo for the random alloys. According to Figure 2b, the weaker NP is the one for 25% Co, having a negative SFE which indicates preferential nucleation of hcp phase. Therefore, tailoring content and topology of the NP one can dial-in plastic yielding.

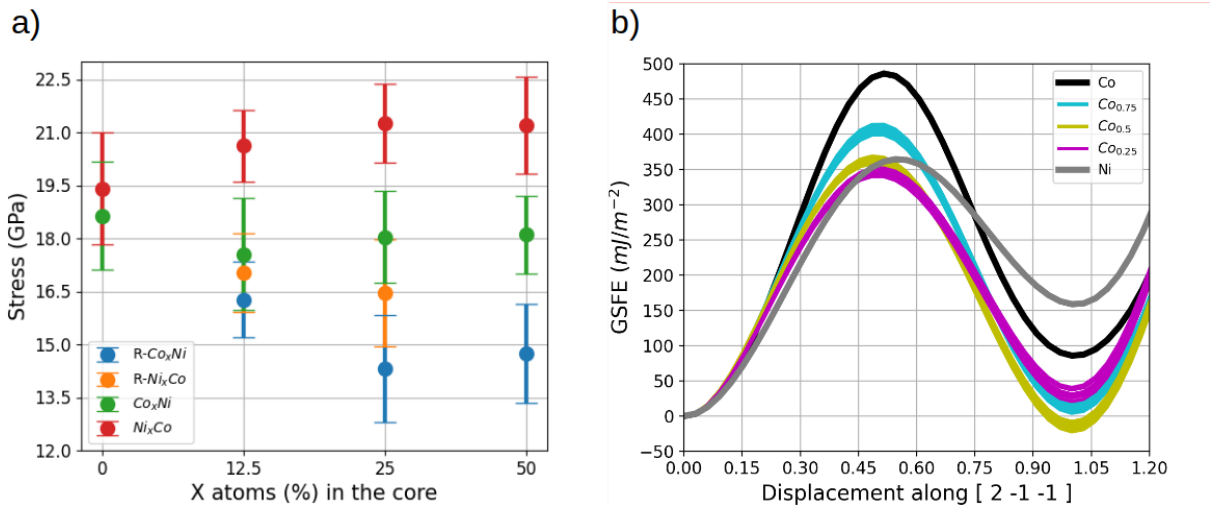

Figure 2. (a) Yield strength versus composition. Average and standard deviation are extracted from 15 simulations of each case. Monometallic Co NP is identified as Ni_0Co, and monometallic Ni NP as Co_0Ni. Core-shell NP with a core of X % of Co atoms are shown as Co_xNi, and NP with a core of X % of Ni atoms as Ni_xCo. Random alloy Co_xNi NP are shown as R-Co_xNi, and random Ni_xCo NP as R-Ni_xCo. (b) Generalized stacking fault energy (GSFE) calculated for a bulk sample with different compositions, for relaxed configurations. For alloys, 10 different random samples are considered, giving some spread in the calculated values.

The deformation mechanism in the monometallic Co NPs is described next in terms of dislocation events. In all cases, the nucleation of Shockley partial dislocations (SPD) occurs at the NP surface. Due to the orientation of the nanoparticle with respect to the indenters, the Schmid factor is the same for all the glide planes[10], and thus dislocations are likely to occur on any of them. The propagation of such SPD in the fcc crystalline structure leaves a stacking fault behind, and two planes of atoms at the stacking fault are identified as having hcp structure. This SPD does not propagate across the NP nor vanishes at the NP surface because other SPD nucleates at the surface, in another glide plane, and collides with the previous SPD forming a sessile Hirth dislocation. In a force-strain curve, the plastic region is reached when dislocations appear for the first time in the NP. This occurs in Figure 3a at a strain of 3.64%. A steep decrease in the force can be found (marked as a blue stripe in Figure 3a) due to the nucleation of dislocations at the top surface. During the nucleation process, other SPD are nucleated at the surface and an incomplete pyramid composed of Hirth and Shockley partial dislocations is formed (Figure 3b). As nanoindentation continues, other SPD nucleate and form a stacking fault pyramid (SFP). The dislocation density due to the appearance of a single SFP is approximately $1.5*10^{16}$ m^{-2}. The appearance of SFP after the elastic regime is by far the most common feature when plastic deformation occurs, not only in monometallic nanoparticles. In our simulations, the appearance of complete SFP on both poles was observed in monometallic, core-shell nanoparticles (except for $Co_{50}Ni_{50}$), and random nanoalloys with 12.5 and 87.5% of Co atoms. On the other occasions, a triangular prism structure appears instead of the SFP, with a short dislocation line connecting two triangular faces. We note that the increase in the indentation force in the plastic regime is due to the concentration of sessile dislocations at the poles, allowing a maximum force which nearly doubles the force at yielding. Similar structures have been observed for pure Ni NP[10] and for other metallic NP.[17]

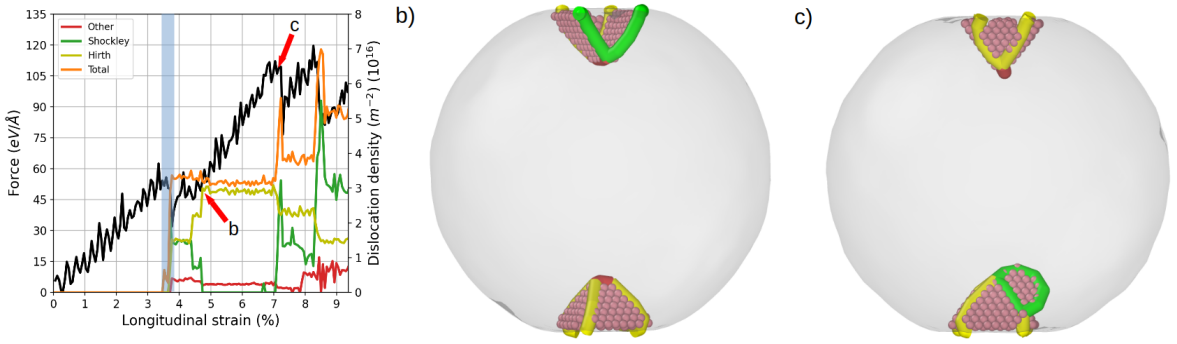

Figure 3. (a) Force vs- longitudinal strain (black line) and dislocation density (orange line) of a monometallic Co NP. Shockley partials, Hirth, and unknown ("other") dislocation densities are indicated by green, yellow, and red lines, respectively. Snapshots taken at: (b) 7.04% and (c) 7.1% longitudinal strain, from different viewpoints. Shockley partial, Hirth, and Other dislocation are represented by a green, yellow, and red lines, respectively; Co hcp atoms are represented by pink spheres, and fcc atoms are omitted for clarity.

The mechanical response of the different studied systems was followed by dislocation analysis with DXA. Figure 4a shows the force vs- longitudinal strain curve and total dislocation density for a $Co_{50}Ni_{50}$ with a core-shell distribution. Several snapshots, taken at different strains, showing the formation of stacking faults and the associated propagation of SPD across the NP (from the SFP towards the opposite NPs surface) are shown in Figures 4b-e. In Fig. 4b, the dislocations nucleated at the surface form a stable structure that provokes hardening; this is a stage immediately before the nucleation of another Shockley partial dislocation that lowers the overall stress of the particle. As it can be noted in Fig. 4c, this dislocation nucleates from one of the faces of the pyramid. The propagation of this dislocation leaves a stacking fault behind, until the dislocation vanishes at the surface of the NP, as can be seen in Fig. 4d. In the same figure, it can be noted that at the north pole of the NP an SPD nucleates on the surface, forming an extrinsic SF that leads to a nanotwin; this twin can be seen completely formed in Fig. 4e. It is worth noting that we only observed the generation of twins in core-shell structures, mostly in CoNi NP (see also SI for core-shell structures with other compositions). Finally, in Fig. 4d we can see the nucleation of a partial dislocation on the plane next to the nanotwin. The partial is initially pinned, and then starts propagating further, with some small advance shown in Fig. 4e.

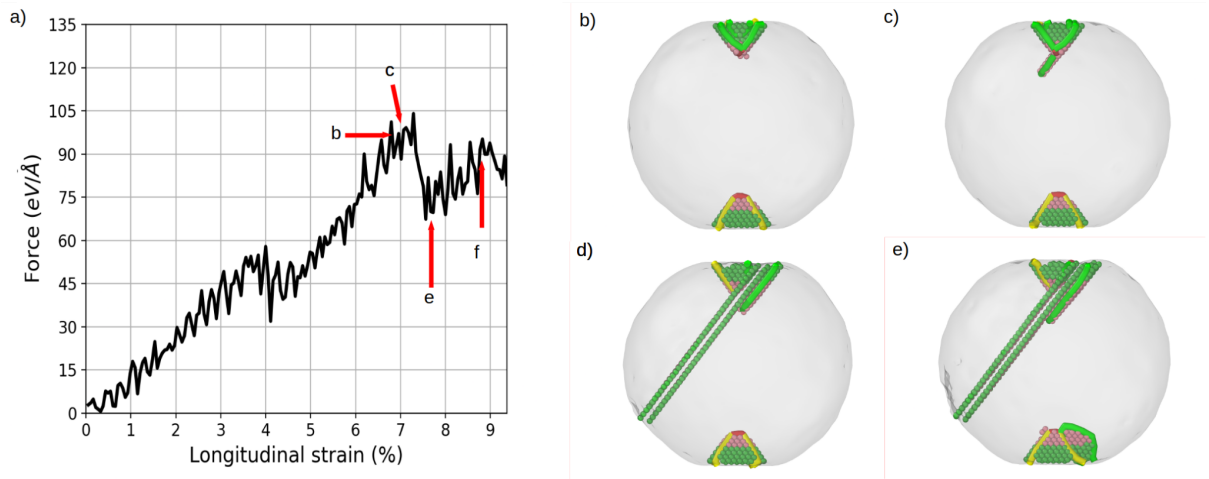

Figure 4. (a) Force-strain curve of core-shell $Co_{50}Ni_{50}$. Snapshots taken at: (b) 6.96%, (c) 7.12%, (d) 7.67%, and (e) 8.71% longitudinal strain. Shockley partial, Hirth, and Other dislocation are represented by a green, yellow, and red lines, respectively; Co hcp atoms are represented by pink spheres, whereas Ni hcp atoms are represented by green spheres, while fcc atoms are omitted for clarity.

When the composition of core and shell are inverted, and now the core is composed of Ni and the shell of Co, the nucleation of SPD proceeds on the surface of the NP just as in the CoNi nanoparticles, with the nucleation of dislocations forming the pyramidal structures at the poles of the NP, as shown in Fig. 5b, which corresponds to the point when hardening ends, labeled as (b) in the force-strain curve of Fig. 5a. One of the Hirth dislocations that form the pyramid dissociates into

two Shockley partials. As can be seen in Fig. 5c, one of the SPD remains at the edge of the pyramid while the other propagates leaving a stacking fault behind. In Fig. 5d, there are four SPD that were dissociated from two Hirth dislocations, propagating on different slip planes. Dislocation reactions lead to SPD propagation towards the surface near the north pole, leading to the absorption of the SPD by the surface in Fig. 5e.

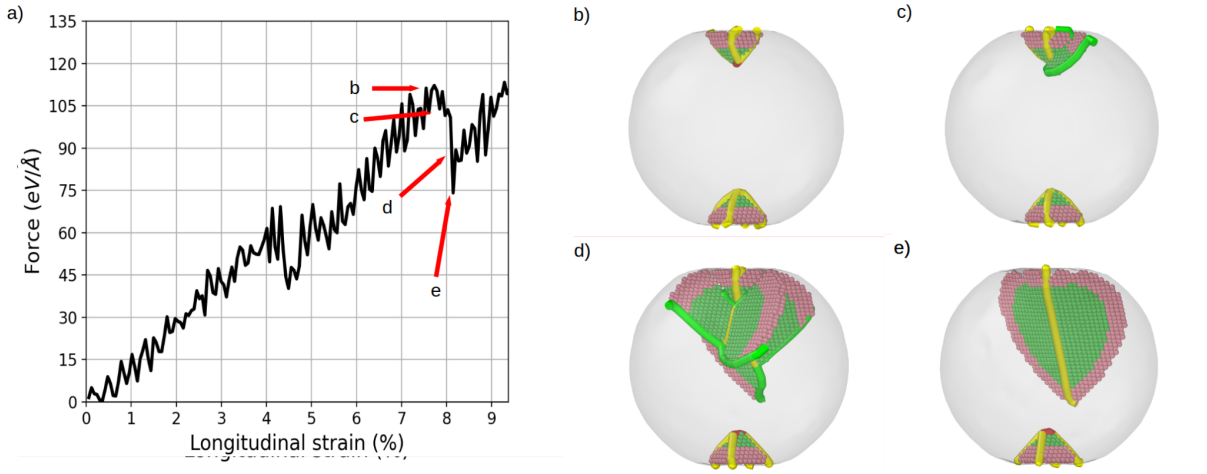

Figure 5. (a) Force-strain curve of core-shell $Ni_{50}Co_{50}$. Snapshots taken at: (b) 7.72%, (c) 7.84%, (d) 8.02%, and (e) 8.14% of longitudinal strain. Shockley partial, Hirth, and Other dislocation are represented by a green, yellow, and red lines, respectively; Co hcp atoms are represented by pink spheres, whereas Ni hcp atoms are represented by green spheres, while fcc atoms are omitted for clarity.

Finally, NP with randomly distributed atoms are studied, and the equiatomic alloy case is shown in Fig. 6. As in the core-shell structures, the SPDs nucleate at the surface and form a pyramid on each of the poles (Fig. 6b). As was observed in the $Ni_{50}Co_{50}$ core-shell nanoparticle, Hirth dislocations dissociate into two SPD (Fig. 6c). SPD propagates and reaches the surface, leaving behind SF planes and a long Hirth dislocation (Fig. 6d). Additional SF propagation from pyramid faces is shown in Fig. 6e.

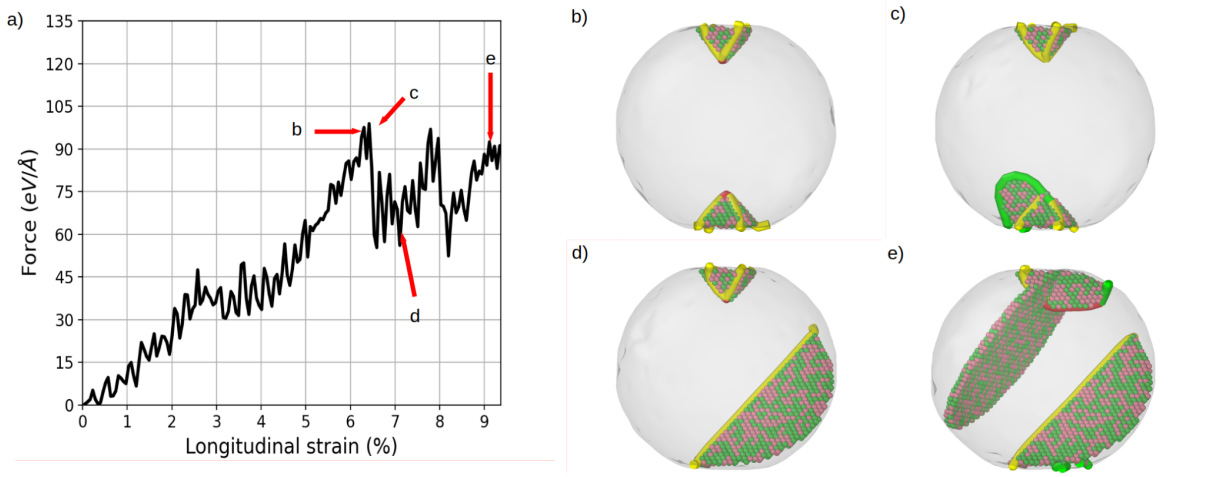

Figure 6. (a) Force-strain curve of random $Co_{50}Ni_{50}$. Snapshots at: (b) 6.36%, (c) 6.42%, (d) 7.05%, and (e) 9.17% of longitudinal strain. Shockley partial, Hirth, and Other dislocation are represented by a green, yellow, and red lines, respectively; Co hcp atoms are represented by pink spheres, whereas Ni hcp atoms are represented by green spheres, while fcc atoms are omitted for clarity.

Summary and conclusions:

The mechanical response under nanoindentation of pure Co and Ni NPs as well core−shell and random mixed NiCo nanoalloys was studied using MD simulations.
The topology of the nanoalloy strongly affects mechanical response. Plasticity is dominated by Shockley partial dislocations (SPD). Independently of the elemental distribution, nucleation of SPD starts at the NP surface. The nucleated SPDs could lead to the formation of a stacking fault pyramid (SFP); the appearance of SFP during compression is more likely in core-shell nanoparticles than in random nanoalloys.

From the alloys studied, NiCo core-shell nanoalloys present the highest yield strength, that is, the maximum resistance to produce plastic deformation. This is understood by the fact that Co presents the highest unstable stacking fault energy; since USFE is related to dislocation nucleation barriers, a high concentration of Co at the surface, where SPD are nucleated, will increase the yield strength of the nanoparticle. From this observation, it is expected that, if the hardest materials are used as shells, the mechanical resistance against external forces will be increased.

The present study also reveals that the elastic response is not strongly correlated to the elemental distribution for NiCo nanoalloys. However, these results could change if the metals forming the alloy are selected with more pronounced differences in their mechanical properties.

In contrast with our previous work[5], where we studied the mechanical response of AuPd core-shell nanoalloys under indentation, where we observed nucleation of partial dislocation at the interface between both metals, here we observed that nucleation of SPD always occurs at the NP surface. This phenomenon could be understood in terms of the small lattice match between Co and Ni (Co: a=3.52 Å, Ni: a=3.5 Å), while, in AuPd alloys, the lattice mismatch is close to 5% and promotes the nucleation of dislocations at the interface.

We believe that the use of molecular simulations to investigate the deformation mechanisms in metal nanoparticles may play an important role in the design of nanoalloys for specific purposes. In future studies we contemplate adding an additional element to form a medium entropy alloy, such as NiCoCr[21]. Predicting the behavior of individual nanoparticles of this kind under an external force using MD simulations, and possibly guided by electron microscopy observations, can help tailor nanoparticle mechanical properties for technological applications.

Acknowledgments

The authors thank financial support from Consejo Nacional del Investigaciones en Ciencia y Tecnología (CONICET) through Grant PIP 11220200101385CO, FONCyT PICT-A-2020-2943, and SeCyT-UNC Program PAGE#1. Computational resources were provided by Centro de Cómputo de Alto Desempeño (CCAD-UNC), Universidad Nacional de Córdoba (http://ccad.unc.edu.ar/), and Laboratorio Nacional de Supercómputo del Sureste de México (http://lns.org.mx). This work has been partially carried out with resources provided by the CYTED cofounded Thematic Network RICAP (517RT0529). S.J.M.R. acknowledges the support from UANL through the PAICYT CE1650-21 grant. E.M.B. acknowledges the support from a SIIP-UNCuyo 2022-2023 grant and FONCyT PICTO-UUMM-2019-00048. JAdlRA thanks CONICET for a fellowship.

References:

(1) Uchic, M. D.; Dimiduk, D. M.; Florando, J. N.; Nix, W. D. Sample Dimensions Influence Strength and Crystal Plasticity. *Science* **2004**, *305* (5686), 986–989. https://doi.org/10.1126/science.1098993.

(2) Greer, J. R.; De Hosson, J. Th. M. Plasticity in Small-Sized Metallic Systems: Intrinsic versus Extrinsic Size Effect. *Progress in Materials Science* **2011**, *56* (6), 654–724. https://doi.org/10.1016/j.pmatsci.2011.01.005.

(3) Mordehai, D.; Lee, S.-W.; Backes, B.; Srolovitz, D. J.; Nix, W. D.; Rabkin, E. Size Effect in Compression of Single-Crystal Gold Microparticles. *Acta Materialia* **2011**, *59* (13), 5202–5215. https://doi.org/10.1016/j.actamat.2011.04.057.

(4) Kiani, M. T.; Wang, Y.; Bertin, N.; Cai, W.; Gu, X. W. Strengthening Mechanism of a Single Precipitate in a Metallic Nanocube. *Nano Lett.* **2019**, *19* (1), 255–260. https://doi.org/10.1021/acs.nanolett.8b03857.

(5) de la Rosa Abad, J. A.; Londoño-Calderon, A.; Bringa, E. M.; Soldano, G. J.; Paz, Sergio. A.; Santiago, U.; Mejía-Rosales, S. J.; Yacamán, M. J.; Mariscal, M. M. Soft or Hard? Investigating the Deformation Mechanisms of Au–Pd and Pd Nanocubes under Compression: An Experimental and Molecular Dynamics Study. *J. Phys. Chem. C* **2021**, *125* (45), 25298–25306. https://doi.org/10.1021/acs.jpcc.1c07685.

(6) Guo, D.; Xie, G.; Luo, J. Mechanical Properties of Nanoparticles: Basics and Applications. *J. Phys. D: Appl. Phys.* **2014**, *47* (1), 013001. https://doi.org/10.1088/0022-3727/47/1/013001.

(7) Davis, J. R.; others. *Nickel, Cobalt, and Their Alloys*; ASM international, 2000.

(8) Sharma, A.; Hickman, J.; Gazit, N.; Rabkin, E.; Mishin, Y. Nickel Nanoparticles Set a New Record of Strength. *Nat Commun* **2018**, *9* (1), 4102. https://doi.org/10.1038/s41467-018-06575-6.

(9) Bian, J.-J.; Wang, G.-F. Atomistic Deformation Mechanisms in Copper Nanoparticles. *j comput theor nanosci* **2013**, *10* (9), 2299–2303. https://doi.org/10.1166/jctn.2013.3201.

(10) Goryaeva, A. M.; Fusco, C.; Bugnet, M.; Amodeo, J. Influence of an Amorphous Surface Layer on the Mechanical Properties of Metallic Nanoparticles under Compression. *Phys. Rev. Materials* **2019**, *3* (3), 033606.

https://doi.org/10.1103/PhysRevMaterials.3.033606.
(11) Thompson, A. P.; Aktulga, H. M.; Berger, R.; Bolintineanu, D. S.; Brown, W. M.; Crozier, P. S.; in 't Veld, P. J.; Kohlmeyer, A.; Moore, S. G.; Nguyen, T. D.; Shan, R.; Stevens, M. J.; Tranchida, J.; Trott, C.; Plimpton, S. J. LAMMPS - a Flexible Simulation Tool for Particle-Based Materials Modeling at the Atomic, Meso, and Continuum Scales. *Computer Physics Communications* **2022**, *271*, 108171. https://doi.org/10.1016/j.cpc.2021.108171.
(12) Brown, W. M.; Wang, P.; Plimpton, S. J.; Tharrington, A. N. Implementing Molecular Dynamics on Hybrid High Performance Computers – Short Range Forces. *Computer Physics Communications* **2011**, *182* (4), 898–911. https://doi.org/10.1016/j.cpc.2010.12.021.
(13) Li, Q.-J.; Sheng, H.; Ma, E. Strengthening in Multi-Principal Element Alloys with Local-Chemical-Order Roughened Dislocation Pathways. *Nat Commun* **2019**, *10* (1), 3563. https://doi.org/10.1038/s41467-019-11464-7.
(14) Stukowski, A. Visualization and Analysis of Atomistic Simulation Data with OVITO–the Open Visualization Tool. *Modelling and Simulation in Materials Science and Engineering* **2009**, *18* (1), 015012. https://doi.org/10.1088/0965-0393/18/1/015012.
(15) Larsen, P. M. Robust Structural Identification via Polyhedral Template Matching. **2016**, 18.
(16) Stukowski, A.; Bulatov, V. V.; Arsenlis, A. Automated Identification and Indexing of Dislocations in Crystal Interfaces. *Modelling Simul. Mater. Sci. Eng.* **2012**, *20* (8), 085007. https://doi.org/10.1088/0965-0393/20/8/085007.
(17) Amodeo, J.; Pizzagalli, L. Modeling the Mechanical Properties of Nanoparticles: A Review. *Comptes Rendus. Physique* **2021**, *22* (S3), 1–32. https://doi.org/10.5802/crphys.70.
(18) Jarlöv, A.; Ji, W.; Zhu, Z.; Tian, Y.; Babicheva, R.; An, R.; Seet, H. L.; Nai, M. L. S.; Zhou, K. Molecular Dynamics Study on the Strengthening Mechanisms of Cr–Fe–Co–Ni High-Entropy Alloys Based on the Generalized Stacking Fault Energy. *Journal of Alloys and Compounds* **2022**, *905*, 164137. https://doi.org/10.1016/j.jallcom.2022.164137.
(19) Van Swygenhoven, H.; Derlet, P. M.; Frøseth, A. G. Stacking Fault Energies and Slip in Nanocrystalline Metals. *Nature Materials* **2004**, *3* (6), 399–403. https://doi.org/10.1038/nmat1136.
(20) Smith, L.; Farkas, D. Connecting Interatomic Potential Characteristics with Deformation Response in FCC Materials. *Computational Materials Science* **2018**, *147*, 18–27. https://doi.org/10.1016/j.commatsci.2018.01.055.
(21) Wang, W.; Hua, D.; Luo, D.; Zhou, Q.; Li, S.; Shi, J.; Wang, H. Molecular Dynamics Simulation of Deformation Mechanism of CoCrNi Medium Entropy Alloy during Nanoscratching. *Computational Materials Science* **2022**, *203*, 111085. https://doi.org/10.1016/j.commatsci.2021.111085.